Mechanism of salinity change and hydrogeochemical evolution of groundwater in the Machile-Zambezi Basin, South-western Zambia

Kawawa E. Banda[a,b*], Wilson Mwandira[b], Rasmus Jakobsen[c], Jason Ogola[a], Imasiku Nyambe[b], Flemming Larsen[c]

[a]Department of Mining and Environmental Geology, *University of Venda*, Thohoyandou, 0950, South 7 Africa.
b Integrated Water Resources Management Centre/Department of Geology, *University of Zambia* - C/O School of Mines, Lusaka, Zambia.
[c]Department of Geochemistry, *Geological Survey of Denmark and Greenland (GEUS)*, 10, Øster 11 Voldgade, DK-1350 Copenhagen K, Denmark.

* Corresponding author: Tel.: +260 77533041, Email address: Kawawa.Banda@unza.zm

Abstract
Machile-Zambezi Basin, South-Western Zambia hosts high salinity groundwater which threatens water security for rural inhabitants. This study investigates the hydrological mechanism that led to high salinity and the geochemical evolution of the groundwater system. The Machile-Zambezi Basin is part of the wider Kalahari Basin which underwent major palaeo-environmental climatic, tectonic and sedimentology dynamics which must have impacted the groundwater salinity. The study examines the groundwater level, hydrochemistry, environmental isotopes ($^{18}O/^{16}O$, $^{2}H/^{1}H$, $^{3}H/^{3}He$, $^{14}C/^{13}C$). In addition, the sediment cation exchange capacity (CEC) and pore-water chemistry on intact core material were measured. The groundwater chemistry evolved from fresh $Ca(Na)HCO_3$ to saline $Na(Ca, Mg)SO_4$ due to dissolution of salts and not evaporation as indicated by stable isotopes. The saline groundwater is old with ^{14}C ages estimates of more than 1000 years old and stagnant. Geochemical modelling using PHREEQC suggests that ionic exchange due to release of cations from dissolving salts and sulphate reduction were also important processes in this system. High groundwater salinity is therefore associated with Pre-Holocene environmental changes and is restricted to a stagnant saline zone. It will therefore remain unflushed as long as current climatic conditions remain.

Keywords: *Groundwater; Isotopes; Kalahari; Machile-Zambezi; PHREEQC; Salinity*

HIGHLIGHTS

- Salinity change occurred during the last *pluvial* climatic event, 1000 – 4000 yrs BP
- High salinity groundwater was due to dissolution/leaching of evaporite salts
- PHREEQC modelling suggests ionic exchange and sulphate reduction additionally
- Saline groundwater seems stagnant and does not undergo post depositional dilution

1. Introduction

In arid and semi-arid regions, such as the Kalahari Basin, sustainable exploitation of available groundwater resources is almost impossible without adequate knowledge of the spatial distribution of fresh and saline groundwater and processes that determine their variability (Bouchaou et al., 2008). The Kalahari Basin presents an ideal setting to examine the geochemical evolution of groundwater as factors that may complicate such an evaluation are either minute or not important, for example, aquifer rocks are siliceous and devoid of carbonates, lateral flow is minimal both on the surface and subsurface, and interference by man is still small. The resulting groundwater chemistry is therefore a function of the general geology, degree of chemical weathering of the various rocks and inputs from sources other than water-rock interactions (Domenico, 1972) as well as tectonics, past climatic events and sedimentology. Knowledge of the groundwater residence time is therefore essential to assess the potential effects of changes in environmental pressures such as climatics and hydrological dynamics to sustain usable groundwater. Currently, there is limited knowledge on the impacts of palaeoclimatic events on the hydro-geochemistry and timing of salinity change in arid and semi-arid regions especially in Africa.

Water quality studies in the Kalahari Basin, have predominantly been used as a diagnostic tool to investigate the geological occurrence and chemical evolution of groundwater (e.g. Mazor et al., 1980, McCarthy et al., 1991, Linn et al., 2003, Eckardt et al., 2008), and determine recharge rates (e.g. Mazor et al., 1977, De Vries et al., 2000, Wanke et al., 2008, Stadler et al., 2010). However, the palaeo-environmental climate, tectonics and sedimentology (Ringrose et al., 2005, Burrough et al., 2009b) responsible for the formation and subsequent geomorphological development have received little or no attention in the interpretation of hydrochemical processes. Southern Africa, after the breakup of Gondwana, formed a passive continental margin along the coastal margin and a down warped interior basin (Moore, 1999). This altered the drainage pattern of major river systems although major sedimentation only commenced after tectonic-induced flexures along the Etosha-Griqualand-Transvaal (EGT) and Okavango-Kalahari-Zimbabwe (OKZ) fault axes propagated by the East-African Rift System. Consequently, a closed drainage was formed that led to the formation of a large lake system referred to as the Palaeo-Lake Makgadikgadi accumulating flows from the Palaeo-Zambezi, Okavango, Kwando-Linyanti rivers. This lake underwent different lake stages driven by climate and tectonics throughout the Quaternary, impacting the depositional environment (Moore et al., 2012, Matmon et al., 2017). Sediments deposited in this environment were a combination of both aeolian and fluvial-lacustrine. To date, most of this lake has vanished with remnants such as the Makgadikgadi salt pans

(Sua and Ntwetwe saltpans) and the Okavango Delta. A detailed account of these dynamics is given by several authors such as Moore and Larkin (2001), and Thomas and Shaw (2002). Verhagen (1995) postulates that mineralisation of groundwater in the Kalahari Basin is constrained by the aquifer structure which also controls the salinity build-up and/or flushing of the aquifer. This study will investigate the impact of Palaeo-climate on the groundwater hydro-geochemistry and the mechanism of salinity change. The findings will aid in providing information for improved understanding of the hydrological processes that control the evolution of groundwater in the Machile - Zambezi Basin.

2.0 Study area

2.1 Location

The Machile-Zambezi Basin is a sub-basin of the greater Kalahari Basin located in the south-western part of Zambia, southern Africa, covering an area of 26 088 km^2 (Fig. 1). It lies between latitudes 15.98 S and 17.90 S and longitudes 24.09 E and 26.50 E decimal degrees.

2.2 Topography

The study area has a low gradient topography ranging from 930 – 2000 m above mean sea level (amsl) and sloping at an average gradient of 0.6% making it prone to extensive seasonal floods (Chongo et al., 2015). Several streams and rivers drain most of the basin and form seasonal tributaries of the perennial Zambezi River.

2.3 Climate

The climate of Machile-Zambezi Basin can be classified as semi-arid, which is mainly dry except in rainy months (November to March) and characterised by hot-dry summer (April and May; August to October) and cold winter (June to August). Temperatures in the summer rise to 40 ºC and drop to 5 ºC in winter. The mean annual rainfall in the area is 500 mm (Beilfuss, 2012) and mean recharge has been estimated at 10 mm (Wanke et al., 2008). Potential evapotranspiration is estimated in the range 900–1200 mm/year (Stadler et al., 2010).

2.4 Regional Geological Setting

The study area is underlain by the Kalahari Supergroup rocks deposited in a basin stretching approximately 2200 km covering nearly all of Botswana, and stretching to the south into the northern Cape Province of South Africa, to the west into Namibia and to the north into Zambia, Angola and the

Democratic Republic of Congo (Moore et al., 2012). The Kalahari Basin is an epeirogenetic depression, that was probably formed in the Late Cretaceous as a result of downwarp in the interior of the Southern African terrane (Haddon and McCarthy, 2005). The downwarp along with uplift along epeirogenetic axes back-tilted rivers into the newly formed Kalahari Basin, initiating deposition of the Kalahari Supergroup sediments. Initial deposition of basal gravels occurred in the channels of the Cretaceous rivers, with other unsorted gravel beds deposited at the base of scree slopes, along edges of valleys and fault bounded structures. The accumulation of gravels continued as the downwarp of the basin progressed with inter-bedding of the gravel layers with sand and finer sediments carried by the rivers (Haddon and McCarthy, 2005). Thick clay beds accumulated in the lakes that formed as a result of the back-tilting of rivers, with sandstone being deposited in braided streams interfingering with the clays and covering them in some areas as the shallow lakes filled up with sediment (Haddon and McCarthy, 2005). Tectonic activity, which are still ongoing in parts of the Kalahari Basin, have resulted in numerous local stratigraphic variations. Widespread calcretisation and silcretisation of Kalahari Group sediments have further complicated the stratigraphic succession in some areas.

2.5 Geology and Hydrogeology

The local stratigraphy of the study area is shown in Table 1 as described by Money (1972). The sediments are predominantly arenaceous in nature and can be divided into consolidated Karoo layers, which are capped by basaltic lavas (Batoka Basalt), and the overlying younger Kalahari sediments. This study focuses on the Kalahari Supergroup which is further divided into the Barotse and Zambezi Formations. The Barotse Formation, comprises a series of sandstones and quartzites which are subdivided into Lower, Middle and Upper Barotse Members. The Zambezi Formation which rests on the Barotse Formation, consists primarily of loose sand (referred to as the Mongu Sand Member). The formation also includes more recent deposits such as the duricrusts, pod-quartzites, pan limestones, claystones, chertified podzol horizons, saline evaporites, river gravels, flood plain sediments, sheet conglomerates and alluvium. The sediments are essentially fine-grained and are uniform both vertically and laterally (Money, 1972).

Limited hydrogeological information is available for this area and therefore this description is based on available borehole data and a report by Chenov (1978). The main aquifer units of the Kalahari Supergroup are sands and gravel of the Zambezi Formation with a discharge ranging from 3 – 10 L/s. The aquifer systems is composed of a shallow unconfined aquifer of 5 to 60 m thickness with one or

more underlying semiconfined aquifers. The grain size of the aquifer units are well sorted and is in the range of 1.9 to 2.3 Φ (fine sand). Transmissivities range from 10 to 70 m^2/day and a hydraulic conductivity of 1.05 m^2/day (Chenov, 1978). Given that the aquifer system is hosted in a surface deposit, this offers conditions for easy and direct recharge from rainfall infiltration. Groundwater levels are shallow: 1–10 mbs (m below surface) in river valleys and 10 to 15 mbs in interfluve areas. Regional groundwater flow is generally towards river valleys. However, the presence of aquitards prevents the formation of a large extensive aquifer system. Variably developed clay, sandy clay and silty sand, form leaky aquitards and underlying semiconfined aquifer units. Vertical hydraulic conductivity values for aquitards are mostly 10^{-3} to 10^{-4} m/day. The underlying Barotse Formation has massive quartzites and cemented sandstones although fractures are a possible feature. Consequently, this Formation has a low potential as a source of groundwater. The water quality in the Kalahari Supergroup is regarded as fresh although brackish – saline water has been mapped in parts of the basin using geophysics (Sattel and Kgotlhang, 2004, Campbell et al., 2006, Chongo et al., 2015).

3.0 Materials and Methods

3.1 Field Measurements

3.1.1 Groundwater level measurements

Accurate elevation above mean sea level (amsl) and location coordinates of available boreholes were obtained using a differential Trimble (TM) R4-5800 system GPS. Groundwater levels were measured with a Solinst (TM) dip meter. Measurements were taken from the top of the casing pipe as the reference point to the water head. These results from boreholes were then interpolated using the kriging method (Alley, 1993) to produce a groundwater level raster map. The thickness of the unsaturated zone (i.e distance between the land surface and the groundwater) was estimated by subtracting the groundwater table elevation from Shuttle Radar Topographic Mission (SRTM) data. This was done using raster calculator tool in ArcGIS(TM) 10. A detailed description of the methodology is available in Margane and Schuler (2013).

3.1.2 Groundwater sampling

To map the spatial variation of groundwater chemistry, water samples were collected from 34 boreholes as shown in Fig. 1. The boreholes were purged three times before samples were collected. This was done to remove groundwater stored in the well and allow for fresh aquifer water to enter the borehole. Physico-chemical measurement of pH, electrical conductivity (EC) and temperature was done with a

WTW 350i multimeter and alkalinity was determined by Gran titration (Gran, 1952) on site. Samples were collected in 20 mL polyethylene (PE) bottles which were rinsed three times in deionised water prior to dispatch for the field site. Before collection of groundwater samples at each point, sample bottles were rinsed at least three times to ensure the integrity of sample water. Samples for cation analysis were filtered on site through a 0.45µm filter into the bottles and acidified with nitric acid to pH <2 before storage in a cooler box for transportation to the laboratory. Conversely, samples for anion analysis were neither acidified nor filtered after collection, but cooled immediately. In addition to cation and anion water samples, an extra 20 mL of each sample in PE bottles was collected for stable isotope analysis.

Based on the groundwater flow line in Fig. 2, nine boreholes (RV13, RV12-12, RV09, RV08, RV26, RV25, RV37, RV 12-27, RV24) were selected and sampled for tritium-helium ($^{3}H/^{3}He$) and carbon-14 (^{14}C). Samples for $^{3}H/^{3}He$ analysis were collected using a 40 mL copper tubes to prevent any atmospheric interaction as per the sampling protocol described by Weise and Moser (1987). ^{14}C samples were collected in 50 mL PE bottles with tight screw caps to prevent any leakage or atmospheric interaction.

3.1.3 Sediment-core drilling and Geophysical borehole logging

An investigation borehole was drilled at site RV 12 – 27, Kasaya Basic School (Fig. 1) for pore water extraction and cation exchange capacity of sediments. The borehole was drilled to 100 m below ground level (bgl) using a truck-mounted drill rig. Specific samples were selected based on sediment variability. The sediment variability and pore water salinity were further confirmed by gamma and resistivity borehole log using the Robertson ^{TM} resistivity probe. Gamma log profile represents natural gamma ray source that include ^{40}K, ^{238}U and ^{232}Th. Clay– and shale – bearing rocks commonly emit relatively high gamma radiation because they include weathering products of potassium rich feldspars and mica that tend to concrete uranium and thorium by ion absorption and exchange. The resistivity log measures the formation conductivity which is a function of pore water salinity and the void space geometry. Generally, the lower the resistivity the higher the pore water salinity with an exception of certain clay minerals.

3.2. Laboratory analysis

3.2.1 Groundwater Chemistry

Chemical analysis of cations was done using the Perkin Elmer (Analyst 400) Atomic Absorption Spectrometry (AAS) and for anions, using Metrohm Ion Chromatography (IC). Trace elements were analysed using Inductively Coupled Plasma Mass Spectrometry (ICP-MS) at the Geological Survey of Denmark and Greenland (GEUS), Denmark. To check the validity and quality of the chemical analyses, a percentage charge balance error was calculated and this was below 5% for most samples (Table 2). PHREEQC 3.0 (Parkhurst and Appelo, 2013) was used for speciation, calculation of saturation indices and modelling of geochemical processes (dissolution, ionic exchange and sulphate reduction).

3.2.2 Stable isotopes ($^{18}O/^{16}O$ and $^{2}H/^{1}H$)

Stable isotopes of oxygen ($^{18}O/^{16}O$) and hydrogen ($^{2}H/^{1}H$) were measured using the Picarro Cavity Ring – Down Spectrometer (PCRDS) equipped with an autosampler and a vaporiser at GEUS. The results were expressed as ‰ units using the δ (delta) notation with standard deviations not larger than ± 0.2‰ ($\delta^{18}O$) and ± 0.5 ‰ (δD), as calculated from four replicate injections into the vaporiser.

3.2.3 $^{3}H/^{3}He$ and $^{14}C/^{13}C$ analysis

Tritium (^{3}H) and Helium (^{3}He) analysis were conducted at the University of Bremen, Germany, using the Bremen Mass Spectrometer System. ^{3}He was measured from radioactive decay of ^{3}H using an ingrowth method (Sültenfuß et al., 2009); samples were degassed, sealed and stored for 110 days to allow for formation of ^{3}He from the tritium decay. The ^{3}H results were expressed in Tritium Units (TU), and ^{3}He in cubic centimetres at standard temperature and pressure, per kilogram water (cc STP/kg).

$^{14}C/^{13}C$ activity in groundwater samples was analysed at Beta Analytic Limited in Florida. ^{14}C was measured using Accelerator Mass Spectrometry (AMS) and expressed as percentage modern carbon (pmc) while ^{13}C was measured using an Isotope Ratio Mass Spectrometer (IRMS) and expressed as permil (‰) relative to the Pee Dee Belemnite (PDB), with a measurement precision of ± 0.5 ‰. The ^{14}C activity was corrected using $\delta^{13}C$ and the groundwater age calculated using Vogel's model (Vogel, 1970).

3.2.4 Cation Exchange Capacity (CEC)

Adsorbed cations and total cation-exchange capacity (CEC) analysis was based on a method from Appelo and Postma (2005). 1M NH_4Cl solution with a pH of 4.9 was used rather than NaCl to replace adsorbed cations enabling ICP-MS analysis of the desorbed cations. A triplicate analysis of the 1M NH_4Cl solution was made to enable correction for background cations present in the solution. Adsorbed NH_4 was determined by replacing adsorbed NH_4 using a 1M NaCl solution. Total CEC was determined by replacing the adsorbed NH_4 from the first step with Na using 1 M NaCl. To determine adsorbed cations, ten grams of sediment from each of the sampled intervals were immersed in 1M NH_4Cl in a 30 ml Teflon centrifuge tube for one hour. After centrifugation and decanting of the supernatant, the NH_4Cl saturation step was repeated. The supernatant from each step was combined and analysed with ICP-MS for Na, K, Ca, Mg, Al and Fe. Alkalinity and SO_4 were measured on the water from the first replacement step to enable correction for dissolved carbonates and gypsum. The effect turned out to be negligible. Determination of adsorbed NH_4 and total CEC using 1 M NaCl was also carried out with three replacement steps.

3.2.5 Pore-water analysis

Pore-water was extracted using centrifugation as described by Edmunds and Bath (1976) although some of the sediments yielded little or no water. The resulting water sample (~ 2 mls) was filtered through 0.45-µm membrane filters. A saturated paste method was used for the low yielding sediments. This was prepared using the method described by the Non-affiliated Soil Analysis Work Committee - NASWC (1990). The samples were saturated with deionised water to create a saturated paste, and the water was extracted and filtered using centrifugation followed by filtering. The dilution factor introduced was computed as per equation 1:

$$D_f = \frac{\sum S_w + \sum D_w}{\sum S_w}$$

Where: D_f = dilution factor

S_w = Initial soil moisture

D_w = added deionised water (diluent)

The measured concentrations were multiplied by the dilution factor to get actual pore-water concentrations. It is possible however, that some reactions occurred between the sediment and added water during the 'pasting' which could change the water chemistry. A serial extraction experiment gave an indication of gypsum dissolution. Samples were taken at various depths (m) of the drilled core (14, 15, 17, 19, 21, 23, 28, 35, 45, 50) as far as it was possible with the available sampled cores. Pore-water chemical analysis for major cations and anions was done using the Perkin Elmer ICP-MS and Dionex IC, respectively. Physico-chemical measurements of electrical conductivity (EC) were made with a benchtop Hach Radiometer Analytical and CDC 866T Conductivity Cell and pH was measured using a WTW 3310 IDS instrument and electrode. Alkalinity was determined by Gran titration (Gran, 1952).

4.0 Results

4.1 Groundwater flow

Groundwater level and ground elevation were used to generate a piezometric contour map of the study area as shown in Fig. 2. Groundwater flow converges towards the central region of the basin with a thinner unsaturated zone. The hydraulic gradient is 0.002 in the fresh water zone compared to 3.08 x 10^{-4} in the saline zone. The classification of the groundwater into fresh, brackish and saline is presented in section 4.2.

4.2 Groundwater Chemistry

The variability in both physico-chemical measurements and water chemistry analyses is outlined in Table 2. The pH values ranged from 5.3 to 8.3 with most of the values near neutral (7). Dissolved oxygen (DO) concentration ranged from 1.7 to 8.3 mg/L. Water electrical conductivity (EC) measurements were from 12.8 to 23300 µS/cm. The concentration of major cations generally decreased in the order Na > Ca > Mg > K and of anions Cl >SO_4> HCO_3> NO_3. Concentrations span over a large range: cations; Na, 0.52 - 5300 mg/L, Ca, 0.50- 770 mg/L, Mg, 0.10 - 265 and K, 0.41-16.5 mg/L; and for anions; Cl, 0 - 5900 mg/L, SO_4, 0 - 5570 and HCO_3, 0 - 533 mg/L. The samples can be classified into three clusters based on water quality as, fresh – Total Dissolved Solids (TDS) < 1.3 g/L, brackish – 1.3 to 10g/L or saline, > 10 g/L (Fig. 2). The piper plot combined with stiff diagrams (not to scale) differentiates three groundwater types (Fig. 3); fresh groundwater is a Ca-(Na)-HCO_3 water type, whereas the brackish and saline groundwater are Na-HCO_3^- and Na-(Ca, Mg)-SO_4, respectively. PHREEQC speciation and the derived mineral saturation indices, indicate that carbonate and sulphate minerals (calcite, dolomite and gypsum) as shown in Table 2, are the controlling phases, depending on

the water type. Calcite saturation was observed in the majority of the groundwater types. Saline water was saturated or close to saturation with gypsum and dolomite.

4.3. Stable Isotopes

Stable isotope results showed that the majority of fresh groundwaters are clustered on the global meteoric water line (GMWL), $\delta D = 8\delta^{18}O + 10$ (IAEA and WMO, 2006), suggesting recharge from precipitation (Fig. 4). Two fresh groundwater points (RV 24 and RV 36) plot between the GMWL and the evaporation line (EPL). The EPL equation, $\delta D = 5\delta^{18}O - 9.8$, was based on the work of Dincer et al. (1978) in the Okavango Basin. The two points were at the transition zone from fresh to saline water. Brackish groundwater had a δO^{18} ranging from -8 to -3 ‰ and δD between -55 to -30 ‰. The majority of them plot around the GMWL although two points are within margins of error for the EPL (Fig. 4). The saline groundwater had an isotopic signature for δO^{18}, -8 to -5 ‰, and δD, -55 to -40 ‰. These points are not on any line (EPL or GMWL) but rather skewed away (Fig. 4). A plot of the EC with δO^{18} of brackish and saline groundwater (Fig. 5), shows the δO^{18} only ranges between -8 to -5 ‰ compared to a wide range in salinity (1,128 to 23,800 µS/cm).

4.4 Groundwater ages

Results for the $^{3}H/^{3}He$ and $^{14}C/^{13}C$ isotopes along the flow line (shown in green in Fig. 2) are summarized in Table 3. ^{3}H results range from 0.03 - 0.94 TU in the fresh-transition zone and 0.00-0.71 TU within the brackish to saline zone. ^{14}C activity in the fresh-transition zone is 57.3 - 93.2 pmc, whereas in the brackish-saline zone it is 66.3 - 106.2 pmc. Furthermore, $\delta^{13}C$ shows an increasing trend in the fresh-transition zone from -21.5 to -16 and -20.1 to -12.8 in the brackish-saline zone. Corrected ages vary from modern to old water with an age of 3,342 years.

4.5 Gamma and resistivity profile

The investigation borehole was composed of sediment lithologies including mainly sandy-clay, sand and clay (Fig. 6). The entire profile has predominantly high conductivity (more than 300 mS/m, except for the upper 10 m with less than 5 mS/m) and some clay contribution (6 – 36 API) based on the resistivity and gamma log respectively.

4.6 CEC

Table 4 shows the exchangeable cations (Ca, Mg, Na, K, Al, Fe, NH_4) on the sediments, and the total Cation Exchange Capacity given as the sum in meq/100g dry sediment, at different depths from core

samples. Ca, Na and Mg are the dominating ions with 0.51 - 11.0, 0.16 - 7.03 and 0.10 - 3.60 meq/100g respectively. The rest of the ionic species have a low to negligible contribution on the sediments; Fe (0 meq/100g), K (0.05 - 0.48 meq/100g), Al (0.00 - 1.52) and NH_4 (0.00 - 0.20). CEC thus has a wide range from 0.87 - 21.0 meq/100g, with an average of 12.4 meq/100g or ~1 eq/l pore-water, if we assume a porosity of 0.25 of the sediments.

4.7 Pore-water analysis

Pore-water chemistry results are shown in Table 5; most of analyses have an associated electrical balance charge error of < 10%. Hydrochemistry results indicate that cation dominance is Na >> Ca > Mg > K, whereas anion dominance is SO_4 > Cl > HCO_3 >> Br. Sodium concentrations range from 622 to 6,938 mg/L and Ca from 29.6 to 347 mg/L. Sulphate ranges from 373 to 6,798 mg/L compared to chloride with a range of 238 to 5,883 mg/L. Pore-water electrical conductivity (EC) ranges from 2,389 to almost 30,000 µS/cm.

5. Discussion

5.1 Mechanism of Salinity change

Sediments in the saline zone are mainly clay and silty-clay with typically a high porosity but poor permeability. Saline sediments therefore act as a barrier to flow with a high potential for fresh groundwater discharge by overland flow (discharge), especially at the interface region of fresh and saline groundwater. This overland discharge is likely lost to evaporation. This is in agreement with the findings of De Vries (1984), who modelled that the current groundwater level in the Kalahari Basin is a result of water table depletion through discharge since the wet pluvial period. However, in the saline zone the dynamics are different. Generally, the resistivity (Fig. 6), does not vary with an increase or decrease in clay and is relatively constant through depth, suggestive of stagnant non-flushing conditions. The poor correlation between EC and δO^{18} (Fig. 5) suggests evaporation is not the controlling mechanism to groundwater salinity build up. High salinity must therefore be due to dissolution or leaching of mineral salts. All the adjusted ^{14}C pmc values in Table 2 are < 85 pmc except for RV 24, located in close proximity to the perennial Zambezi River and prone to seasonal flooding. Pmc values < 85 have been interpreted in the Kalahari Basin to represent rapid rainfall recharge (Verhagen et al., 1974). De Vries et al. (2000) estimates recharge in the Kalahari Basin to be negligible and approximately < 0.5 mm/yr. Rapid recharge is likely associated with the wet pluvial period reported during desiccation of the Palaeo-lake system. The last wet pluvial period has been estimated to occur between 4000 to 1000 years BP

(Riedel et al., 2014) within the range of our ^{14}C groundwater ages. High salinity is therefore a result of imperfectly flushed sediments with mineral salts during the last wet pluvial period. Since there has been insignificant exchange of water following this period, the groundwater is old and saline because the flow of water through the formation is too small to remove mineral salts completely.

5.2 Geochemical processes in the fresh and saline zone

The Ca-(Na)-HCO_3 fresh water is probably a result of silicate weathering. Groundwater samples (Table 2) along the flow line (Fig. 2), suggests dissolution of alumino–silicates. The source material is lithologies with alumino-silicate minerals that include plagioclase, hornblende, and K-feldspars. Reactions releasing Na^+ and Ca^{2+} are exemplified in these two reactions (Appelo and Postma, 2005);.

Albite

$$2\ Na(AlSi_3)O_8 + 2H_2CO_3 + 3H_2O \rightarrow Al_2Si_2O_5(OH)_4 + 2Na^+ + 4H_4SiO_4 + 2HCO_3^-$$

(Kaolinite)

Anorthite

$$Ca(Al_2Si_2)O_8 + 2H_2CO_3 + H_2O \rightarrow Al_2Si_2O_5(OH)_4 + Ca^{2+} + 2HCO_3^-$$

These silicate reactions are kinetically slow and are probably ongoing. Similar observations were made by Mazor et al. (1980), who suggested that the vast majority of the Kalahari groundwater are composed of Ca-(Na)-HCO_3.

To model and explain our observed chemistry in the saline zone, PHREEQC was used. Conceptually, our findings suggest that the high present-day groundwater salinity is a result of dissolution of evaporite salts formed from intense evaporation of the endorheic Palaeo – Lake Makgadikgadi (Burrough et al., 2009a). These evaporites were subjected to intense leaching which replaced old water with fresh leachate. Water isotopes indicate that evaporation is not affecting the system where little fresh groundwater passes through to dilute the salinity which therefore stays high. According to Krothe and Bergeron (1981), high Na^+ and SO_4^- with low HCO_3^- can be explained by four processes: 1) dissolution of gypsum and dolomite; 2) dissolution of calcite; 3) ion exchange with Na bound to clay, and 4) sulphate reduction. These reactions can be generalised as described in the following:

1) $CaSO_4 + CaMg(CO_3)_2 + 2H^+ \leftrightarrow 2Ca^{2+} + 2HCO_3^- + Mg^{2+} + SO_4^{2-}$

The calcium released from the dissolution of gypsum results in precipitation of calcite and the release of magnesium and sulphate into solution, a process also known as de-dolomitization (Plummer et al., 1990). The saturation of calcium in such a system leads to calcite precipitation and increased concentration of magnesium as the process progresses.

2) Infiltration of groundwater through soil and overburden, will enrich it with CO2 which will dissolve precipitates of calcite:

$$CaCO_3 + CO_2 + H_2O \leftrightarrow Ca^{2+} + 2HCO_3^-$$

3) The presence of clay minerals such as montimorillonite with large amounts of exchangeable sodium from dissolved NaCl evaporates could lead to exchange with cations as follows:

$$Ca^{2+} + 2NaX \leftrightarrow CaX_2 + 2Na^+$$

4) Krothe and Bergeron (1981) also suggest sulphate reduction due to organic matter in the system:

$$CH_2O + 0.5\ SO_4^{2-} \leftrightarrow 0.5\ HS^- + HCO_3^- + 0.5\ H^+$$

The released sulphide will often react with Fe-oxides, such as goethite and form Fe-sulphides, typically pyrite.

In this study, the initial solution chemistry for the PHREEQC model was based on hydrochemistry results from Eckardt et al. (2008) on saltpans from within the Palaeo – Lake Makgadikgadi. This solution was equilibrated with calcite and dolomite at an estimated Na^+ and Cl^- content that is used to initialise the exchanger. Another solution, Solution 2, of similar chemistry and exchanger but in equilibrium with gypsum was also added. A cation-exchange-capacity (CEC) of 1.2 eq/L was used as per our analysis. Two scenarios were modelled, gypsum dissolution with ionic exchange without and with sulphate reduction. Model input data are summarised in Table 6. The model without sulphate reduction was driven by reacting 0.09 moles of gypsum in 10 reaction steps, using the pitzer.dat database to handle the high salinities. In the sulphate reduction model, it was driven by reacting 0.104 moles of gypsum and 0.070 moles of organic matter in 10 reaction steps. Equilibrium with goethite and pyrite was defined and here the pitzer.dat database could not be used, so the standard phreeqc.dat database was used. The PHREEQC code is available via Mendeley Repository (Banda et al., 2018).

The model outputs are compared to groundwater results and pore-water chemistry from sediment cores as shown in Fig. 7. Figure 7a, demonstrates a reasonable model fit to the observed evolution in Ca and

Mg with increasing sulphate (gypsum dissolution) and concomitant ion exchange. The initial exchanger composition influences the estimation of the Na concentration. Model results assuming high Na on the exchanger are most consistent with the observations. This indicates that there has been some dissolution of halite during the pluvial period, but the current concentrations of Na and Cl are in a range indicating that halite is not present anymore. The wide range in the measured distribution of exchangeable cations in our results may be attributed to different mixtures of saline and fresh pore-water. These geochemical processes have probably been going on for a long time leading to increased Ca and Mg concentrations in the groundwater and on the exchanger, depending on variations in freshwater fluxes. Accordingly, the model misfit could be due to varying higher Ca and Mg ions contents on the exchanger. The effect is seen in the model results where the exchanger was initialized with a higher proportion of Ca (Fig. 7a). Furthermore, a misfit in the decrease of alkalinity with increasing sulphate (gypsum dissolution) was observed which is also controlled by the initial composition on the exchanger. Higher P_{CO2} could be due to decomposition of organic matter and/or root respiration (vegetation) and redox processes such as bacterial sulphate reduction (Plummer et al., 1990) which also affects the alkalinity. Sulphate reduction facilitated by organic matter was tested in our model (Fig. 7b), with goethite present, leading to pyrite formation. Compared to the model without sulphate reduction, two moles of organic carbon were added for each extra mole of gypsum added (process 4 reaction). As shown in Fig. 7b, the addition of sulphate reduction leads to improved model performance especially for the Mg and alkalinity prediction. In summary, the observed variation in the Ca, Mg, Na and alkalinity is probably due to gypsum dissolution combined with ionic exchange and sulphate reduction over a long period of time.

6.0 Conclusions

Analysis of groundwater chemistry and environmental isotopes combined with field measurements of groundwater flow and geophysical logging (gamma and resistivity) were used to examine processes that led to high salinity in the groundwater of the Machile-Zambezi Basin. The high salinity appears to be the result of dissolution of mineral salts during the last wet pluvial period from 4000-1000 yr BP. The sediments were partially flushed and resulted in old stagnant saline groundwater system because of poor permeability and current low infiltration rates. PHREEQC modelling further showed that besides dissolution, there is ongoing ionic exchange reactions with a Na-rich exchanger as well as sulphate reduction to produce the present day Na-(Ca, Mg)-SO_4^{2-} type water. Due to the setting and the described hydrogeological history of the system, usable water supply for human consumption in the saline zone is limited.

Acknowledgments

This research was supported by the Danish International Development Agency (DANIDA) in the framework of the project, “Programme to support capacity building in the Water Sector for Zambia”, Phase II. Special thanks to Christina Lynge and Pernille Stockmarr at the Geological Survey of Denmark and Greenland, Department of Geochemistry, for the Cation Exchange Capacity measurements, water chemistry and stable isotope measurements. The authors are also grateful to Jürgen Sültenfuß, University of Bremen, for the Tritium - Helium dating measurements and useful comments. Special thanks also to the anonymous reviewers who helped improve this manuscript.

References

Alley, W. M. 1993. Geostatistical Models. *In:* ALLEY, W. M. (ed.) *Regional ground-water quality.* John Wiley & Sons.

Appelo, C. A. & Postma, D. 2005. *Geochemistry, groundwater and pollution,* Leiden, A.A. Balkema Publishers.

[Dataset] Banda, K., Mwandira, W., Jakobsen, R., Ogola, J., Nyambe, I. & Larsen, F. 2018. Phreeqc codes for gypsum reaction using a Na Exchanger with and without Sulphate Reduction. Mendeley Data. PID 241351.

Beilfuss, R. 2012. *A risky climate for southern African hydro: assessing hydrological risks and consequences for Zambezi River Basin dams,* Berkeley, International Rivers.

Bouchaou, L., Michelot, J., Vengosh, A., Hsissou, Y., Qurtobi, M., Gaye, C., Bullen, T. & Zuppi, G. 2008. Application of multiple isotopic and geochemical tracers for investigation of recharge, salinization, and residence time of water in the Souss–Massa aquifer, southwest of Morocco. *Journal of Hydrology,* 352**,** 267-287.

Burrough, S. L., Thomas, D. S. G. & Bailey, R. M. 2009a. Mega-lake in the Kalahari: A late pleistocene record of the Palaeolake Makgadikgadi system. *Quaternary Science Reviews,* 28**,** 1392-1411.

Burrough, S. L., Thomas, D. S. G. & Singarayer, J. S. 2009b. Late Quaternary hydrological dynamics in the Middle Kalahari: Forcing and feedbacks. *Earth-Science Reviews,* 96**,** 313-326.

Campbell, G., Johnson, S., Bakaya, T., Kumar, H. & Nsatsi, J. 2006. Airborne geophysical mapping of aquifer water quality and structural controls in the Lower Okavango Delta, Botswana. *South African Journal of Geology,* 109**,** 475-494.

Chenov 1978. Groundwater resources inventory of Zambia. Commissioned by UNESCO/NORAD Water Research Project and National Council for Scientific Research, Zambia; Unpublished Report, 129 pages; Lusaka.

Chongo, M., Christiansen, A. V., Tembo, A., Banda, K. E., Nyambe, I. A., Larsen, F. & Bauer-Gottwein, P. 2015. Airborne and ground-based transient electromagnetic mapping of groundwater salinity in the Machile–Zambezi Basin, southwestern Zambia. *Near Surface Geophysics,* 13**,** 383-395.

Chongo, M., Wibroe, J., Staal-Thomsen, K., Moses, M., Nyambe, I., Larsen, F. & Bauer-Gottwein, P. 2011. The use of Time Domain Electromagnetic method and Continuous Vertical Electrical Sounding to map groundwater salinity in the Barotse sub-basin, Zambia. *Physics and Chemistry of the Earth, Parts A/B/C,* 36**,** 798-805.

De Vries, J. J. 1984. Holocene depletion and active recharge of the Kalahari groundwaters — A review and an indicative model. *Journal of Hydrology,* 70**,** 221-232.

De Vries, J. J., Selaolo, E. T. & Beekman, H. E. 2000. Groundwater recharge in the Kalahari, with reference to paleo-hydrologic conditions. *Journal of Hydrology,* 238**,** 110-123.

Dincer, T., Hutton, L. & Kupee, B. 1978. Study, using stable isotopes, of flow distribution, surface-groundwater relations and evapotranspiration in the Okavango Swamp, Botswana. International Atomic Energy Agency, Proc. Ser. SM-228/52.

Domenico, P. A. 1972. *Concepts and models in groundwater hydrology*, McGraw-Hill Inc.

Eckardt, F. D., Bryant, R. G., McCulloch, G., Spiro, B. & Wood, W. W. 2008. The hydrochemistry of a semi-arid pan basin case study: Sua Pan, Makgadikgadi, Botswana. *Applied Geochemistry,* 23**,** 1563-1580.

Edmunds, W. M. & Bath, A. H. 1976. Centrifuge extraction and chemical analysis of interstitial waters. *Environmental Science & Technology,* 10**,** 467-472.

Gran, G. 1952. Determination of the equivalence point in potentiometric titrations (Part II). *Analyst,* 77**,** 661-671.

Haddon, I. G. & McCarthy, T. S. 2005. The Mesozoic–Cenozoic interior sag basins of Central Africa: The Late-Cretaceous–Cenozoic Kalahari and Okavango basins. *J Afr Earth Sci,* 43.
IAEA, W. & WMO, W. 2006. Global Network of Isotopes in Precipitation. *The GNIP database*.
Krothe, N. C. & Bergeron, M. P. 1981. Hydrochemical facies in a tertiary basin in the Milligan Canyon area, southwest Montana. *Groundwater,* 19**,** 392-399.
Linn, F., Masie, M. & Rana, A. 2003. The impacts on groundwater development on shallow aquifers in the lower Okavango Delta, northwestern Botswana. *Environmental Geology,* 44**,** 112-118.
Margane, A. & Schuler, P. 2013. Groundwater Vulnerability in the Groundwater Catchment of Jeita Spring and Delineation of Groundwater Protection Zones Using the COP Method. Technical Cooperation Project Protection of Jeita Spring. BGR Technical Report, No. 7. 133 pp.
Matmon, A., Hidy, A. J., Vainer, S., Crouvi, O., Fink, D., Erel, Y., Team, A., Arnold, M., Aumaître, G., Bourlès, D., Keddadouche, K., Horwitz, L. K. & Chazan, M. 2017. New chronology for the southern Kalahari Group sediments with implications for sediment-cycle dynamics and early hominin occupation. *Quaternary Research,* 84**,** 118-132.
Mazor, E., Bielsky, M., Verhagen, B. T., Sellschop, J. P. F., Hutton, L. & Jones, M. T. 1980. Chemical composition of groundwaters in the vast Kalahari flatland. *Journal of Hydrology,* 48**,** 147-165.
Mazor, E., Verhagen, B. T., Sellschop, J. P. F., Jones, M. T., Robins, N. E., Hutton, L. & Jennings, C. M. H. 1977. Northern Kalahari groundwaters - hydrologic, isotopic and chemical studies at Orapa, Botswana. *Journal of Hydrology,* 34**,** 203-234.
McCarthy, T. S., McIver, J. R. & Verhagen, B. T. 1991. Groundwater evolution, chemical sedimentation and carbonate brine formation on an island in the Okavango Delta swamp, Botswana. *Applied Geochemistry,* 6**,** 577-595.
Money, N. J. 1972. An outline of the Geology of western Zambia. Republic of Zambia: Records of the Geological Survey.
Moore, A. 1999. A reappraisal of epeirogenic flexure axes in southern Africa. *South African Journal of Geology,* 102**,** 363-376.
Moore, A. E., Cotterill, F. P. D. & Eckardt, F. D. 2012. The evolution and ages of Makgadikgadi Palaeo-Lakes: consilient evidence from Kalahari drainage evolution, Botswana. *S Afr J Geol,* 115.
Moore, A. E. & Larkin, P. A. 2001. Drainage evolution in south-central Africa since the breakup of Gondwana. *South African Journal of Geology,* 104**,** 47-68.
NASWC 1990. NASWC (Non-Affiliated Soil Analysis Work Committee), 1990. Handbook of standard soil testing methods for advisory purposes. Pretoria: Soil Science Society of South Africa.
Parkhurst, D. L. & Appelo, C. 2013. Description of input and examples for PHREEQC version 3: a computer program for speciation, batch-reaction, one-dimensional transport, and inverse geochemical calculations. US Geological Survey.
Piper, A. M. 1944. A graphic procedure in the geochemical interpretation of water-analyses. *Transactions, American Geophysical Union,* 25**,** 914-928.
Plummer, L. N., Busby, J. F., Lee, R. W. & Hanshaw, B. B. 1990. Geochemical modeling of the Madison aquifer in parts of Montana, Wyoming, and South Dakota. *Water Resources Research,* 26**,** 1981-2014.
Riedel, F., Henderson, A. C., Heußner, K.-U., Kaufmann, G., Kossler, A., Leipe, C., Shemang, E. & Taft, L. 2014. Dynamics of a Kalahari long-lived mega-lake system: hydromorphological and limnological changes in the Makgadikgadi Basin (Botswana) during the terminal 50 ka. *Hydrobiologia***,** 1-29.
Ringrose, S., Huntsman-Mapila, P., Kampunzu, A. B., Downey, W., Coetzee, S., Vink, B., Matheson, W. & Vanderpost, C. 2005. Sedimentological and geochemical evidence for palaeo-environmental

change in the Makgadikgadi subbasin, in relation to the MOZ rift depression, Botswana. *Palaeogeography Palaeoclimatology Palaeoecology,* 217**,** 265-287.
Sattel, D. & Kgotlhang, L. 2004. Groundwater exploration with AEM in the Boteti area, Botswana. *Exploration Geophysics,* 35**,** 147-156.
Stadler, S., Osenbruck, K., Suckow, A. O., Himmelsbach, T. & Hotzl, H. 2010. Groundwater flow regime, recharge and regional-scale solute transport in the semi-arid Kalahari of Botswana derived from isotope hydrology and hydrochemistry. *Journal of Hydrology,* 388**,** 291-303.
Sültenfuß, J., Roether, W. & Rhein, M. 2009. The Bremen mass spectrometric facility for the measurement of helium isotopes, neon, and tritium in water†. *Isotopes in environmental and health studies,* 45**,** 83-95.
Thomas, D. S. G. & Shaw, P. A. 2002. Late Quaternary environmental change in central southern Africa: new data, synthesis, issues and prospects. *Quaternary Science Reviews,* 21**,** 783-797.
Verhagen, B. T. 1995. Semiarid zone groundwater mineralization processes as revealed by environmental isotope studies. *In:* ADAR, E. M. & LEIBUNDGUT, C. (eds.) *Application of Tracers in Arid Zone Hydrology.* Wallingford: International Association Hydrological Sciences, Volume 232.
Verhagen, B. T., Mazor, E. & Sellschop, J. P. F. 1974. Radiocarbon and tritium evidence for direct rain recharge to ground waters in the northern Kalahari. *Nature,* 249**,** 643-644.
Vogel, J. 1970. Carbon-14 dating of groundwater. *Isotope hydrology,* 1970**,** 225-239.
Wanke, H., Dunkeloh, A. & Udluft, P. 2008. Groundwater recharge assessment for the Kalahari catchment of north-eastern Namibia and north-western Botswana with a regional-scale water balance model. *Water Resources Management,* 22**,** 1143-1158.
Weise, S. & Moser, H. 1987. Groundwater dating with helium isotopes. *Isotope techniques in water resources development. IAEA, Vienna.*
Yemane, K., D, G. & Nyambe, I. 2002. Paleohydrological signatures and rift tectonics in the interior of Gondwana documented from Upper Permian lake deposits, the mid-Zambezi Rift basin, Zambia. *In SEPM Special Publication No. 73 on Sedimentation in Continental Rifts,* SEPM (Society for Sedimentary Geology)**,** ISBN 1-56576-082-4, pp. 143-162.

Figure captions

Figure 1: Surface geology of the Machile-Zambezi Basin (modified fromYemane et al., 2002) and the sampled sites. Water chemistry within the 945 m asl proxy shoreline has saline groundwater according to Chongo et al. (2011).

Figure 2: Thickness of the unsaturated zone map with a surficial water table within the topographic low region and the river channels suggesting groundwater loss through these channels and evaporation in the dry season. Environmental isotopes samples were along the green line.

Figure 3: Piper Diagram (Piper, 1944) and Stiff diagram showing distinct groundwater types in the Machile-Zambezi River Basin.

Figure 4: A plot of stable isotope (δD and $\delta^{18}O$) from groundwater samples within the Machile-Zambezi Basin.

Figure 5: Graph of $\delta^{18}O$ and EC for brackish and saline water from the Machile-Zambezi Basin.

Figure 6: Investigation borehole drilled at RV 12 – 27 showing the geological variability and geophysical log (gamma and resistivity).

Figure 7: (a) PHREEQC modelled Ca, Mg and Na with exchangers rich in Ca and Na plotted with observed pore water chemistry and groundwater at Kasaya site. Alkalinity with Na and Ca exchanger as a function of sulphate concentration with no sulphate reduction is also plotted. (b) PHREEQC modelled Ca, Mg, Na with a high Na exchanger and sulphate reduction plotted with pore-water and groundwater chemistry at Kasaya site. Alkalinity is also plotted with the same processes.

Table Captions

Table 1: Stratigraphy of Western Zambia (modified from Money, 1972).

Table 2: Hydrochemistry results over the sampled boreholes in the Machile-Zambezi Basin highlighting low (fresh) salinity and high salinity (brackish and saline) water.

Table 3: Shows the isotope results for tritium – helium and C-14 analysis.

Table 4: Cation Exchange Capacity (CEC) of samples from the investigation borehole (RV 12-27) at sampled depths

Table 5: Pore-water composition of the sediment core samples from the investigation borehole (RV 12-27). SPE refers to saturated paste extraction where centrifugation yielded little or no pore-water.

Table 6: PHREEQC input data to model sulphate dissolution and ionic exchange with and without sulphate reduction.

Figure 1

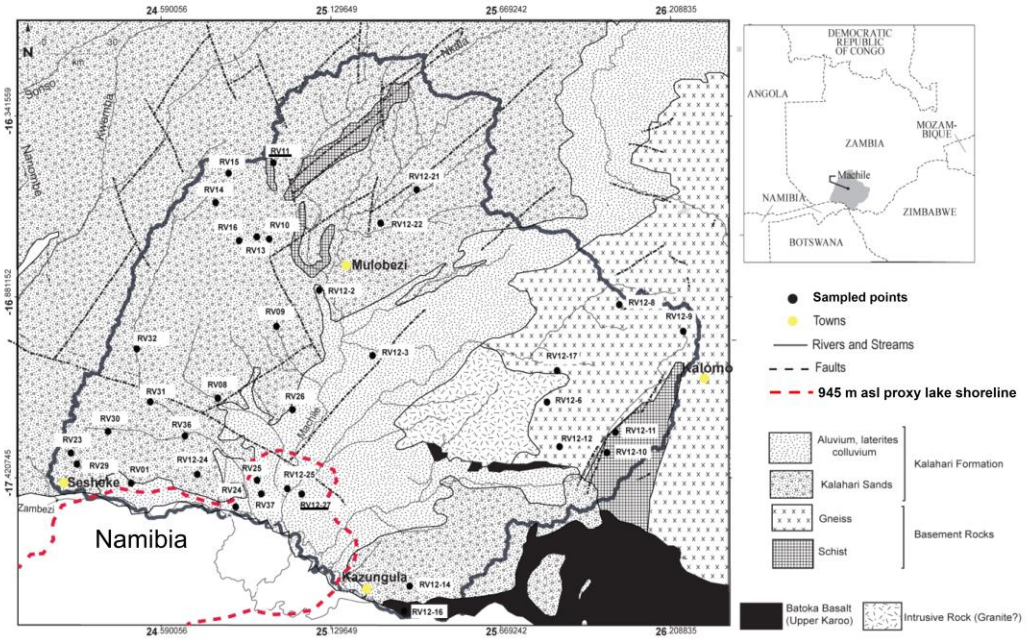

Figure 2

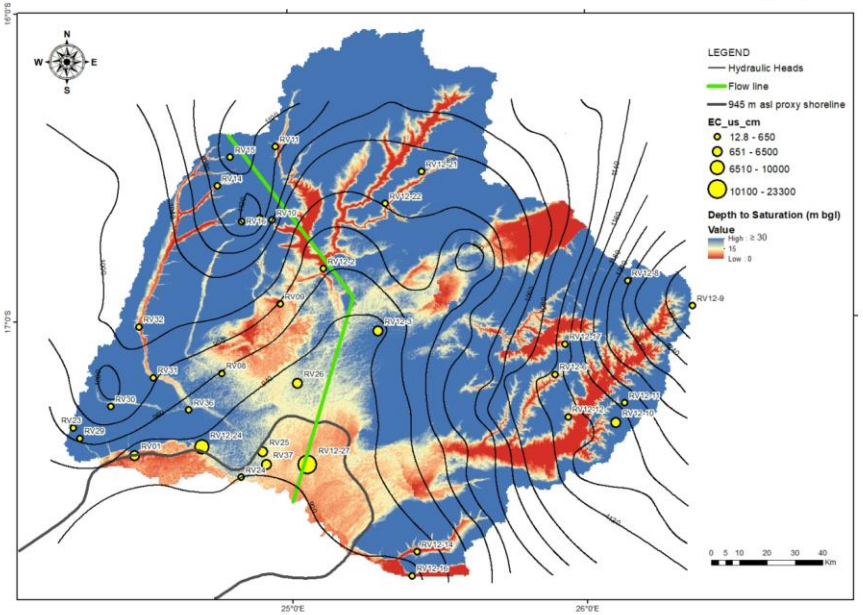

Figure 3

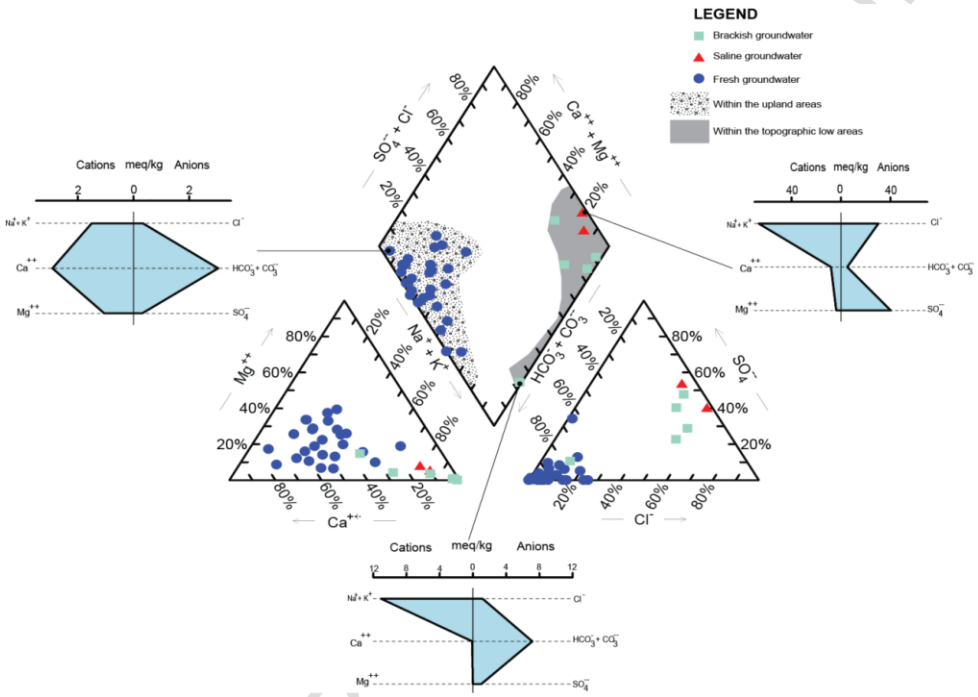

Figure 4

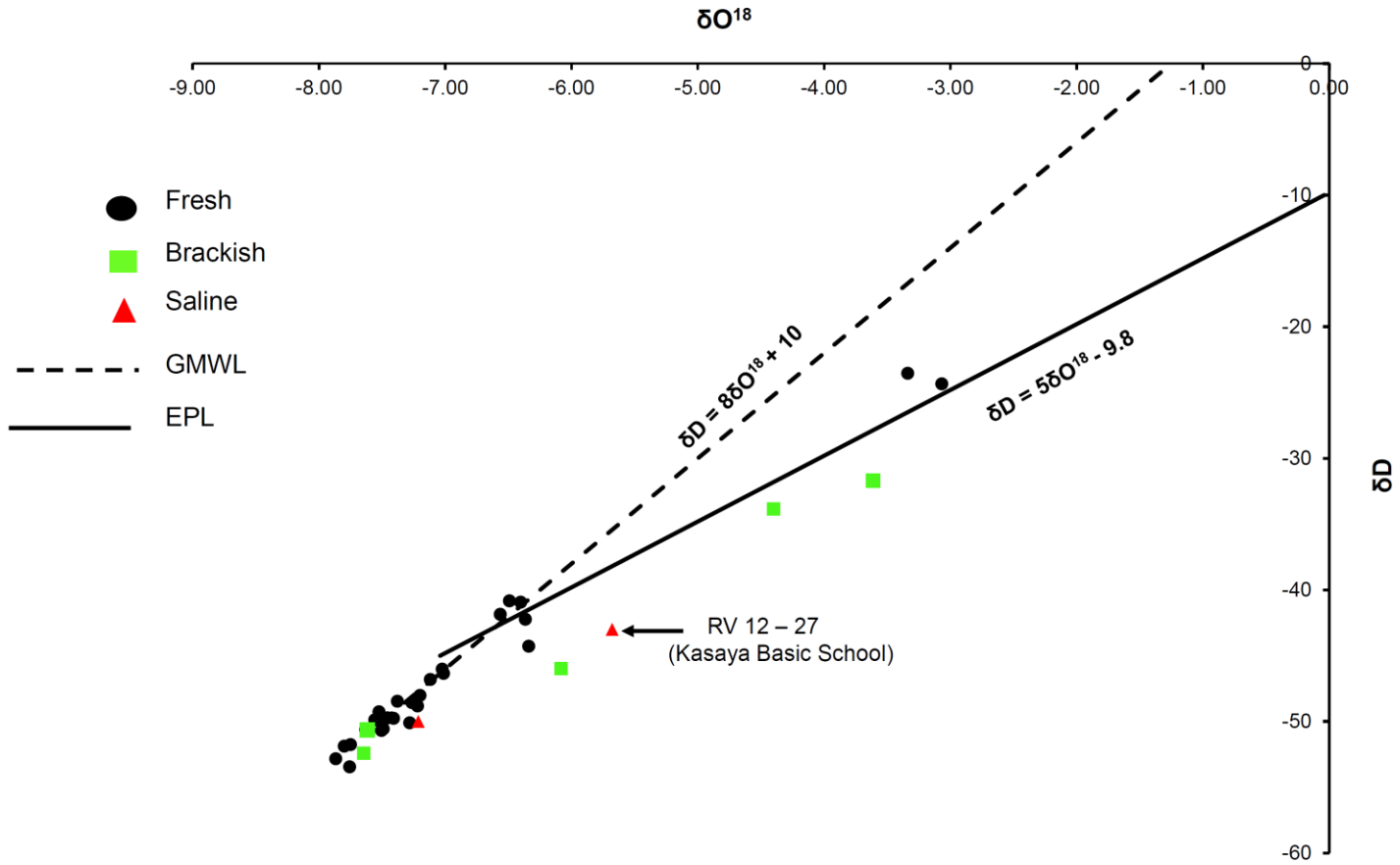
δO18
-9.00
-8.00
-7.00
-6.00
-5.00
-4.00
-3.00
-2.00
-1.00
0.00
0
-10
-20
-30
-40
-50
-60
δD
Fresh
Brackish
Saline
GMWL
EPL
δD = 8δO18 + 10
δD = 5δO18 - 9.8
RV 12 – 27
(Kasaya Basic School)

Figure 5

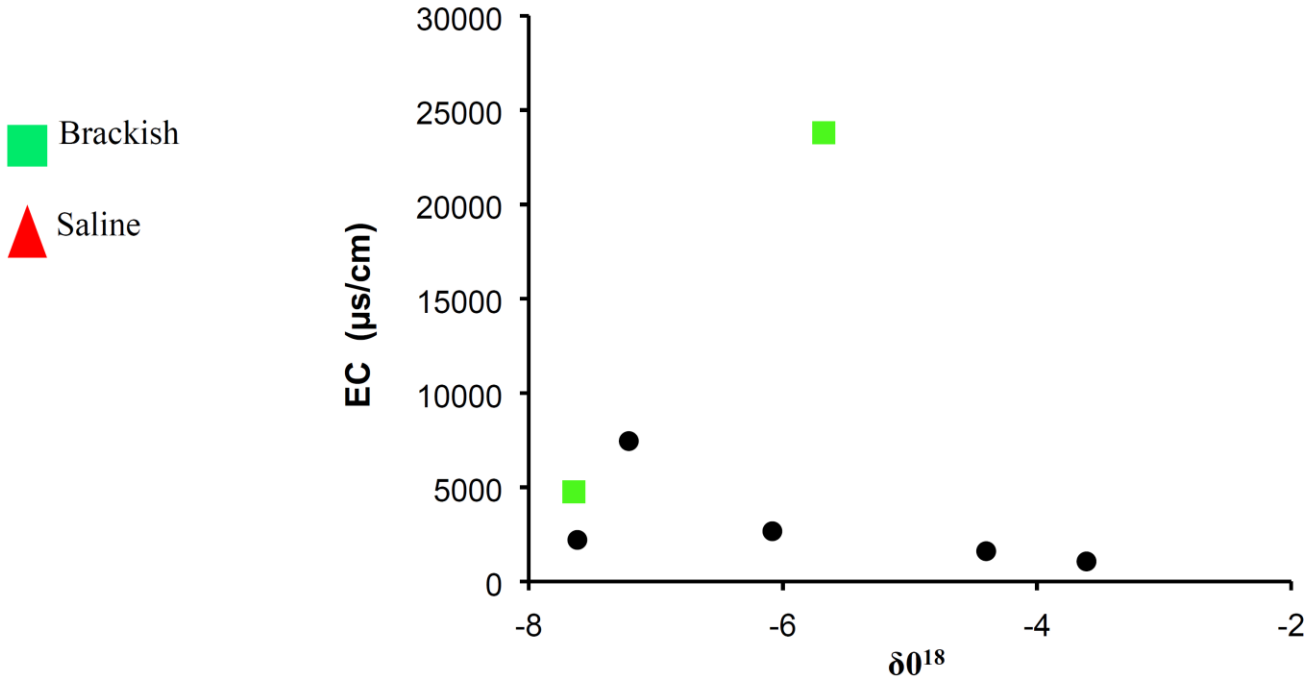
Brackish
Saline
30000
25000
20000
15000
10000
5000
0
EC (µs/cm)
-8
-6
-4
-2
δ0¹⁸

Figure 6

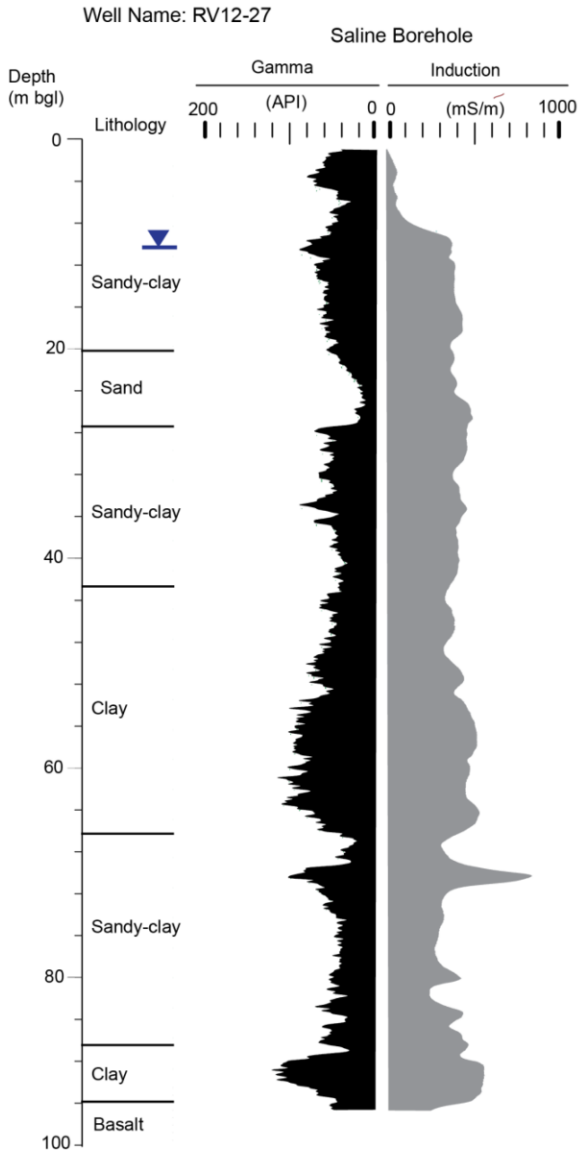
Well Name: RV12-27
Saline Borehole
Depth
(m bgl)
Lithology
Gamma
(API)
200
0
Induction
0
(mS/m)
1000
0
20
40
60
80
100
Sandy-clay
Sand
Sandy-clay
Clay
Sandy-clay
Clay
Basalt

Figure 7

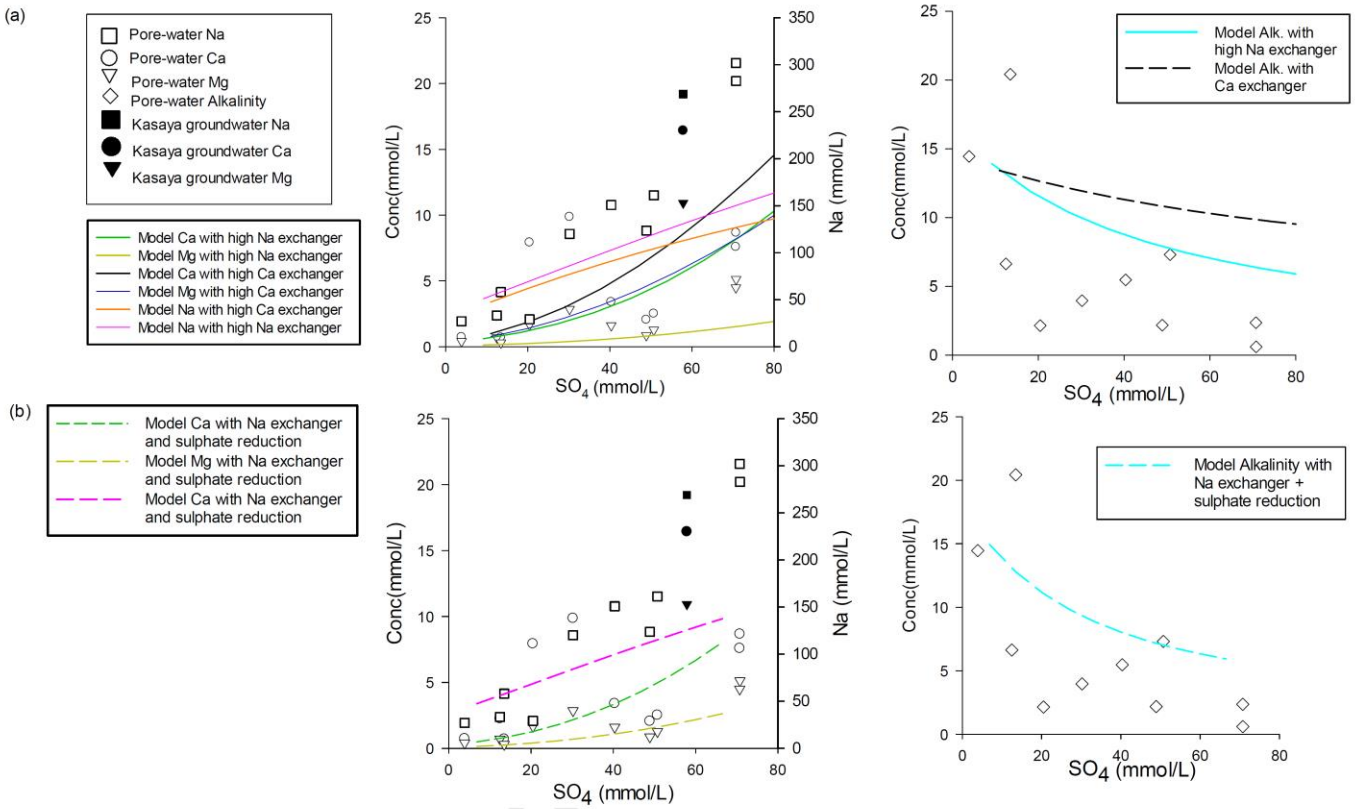
(a)
Pore-water Na
Pore-water Ca
Pore-water Mg
Pore-water Alkalinity
Kasaya groundwater Na
Kasaya groundwater Ca
Kasaya groundwater Mg
Model Ca with high Na exchanger
Model Mg with high Na exchanger
Model Ca with high Ca exchanger
Model Mg with high Ca exchanger
Model Na with high Ca exchanger
Model Na with high Na exchanger
Conc(mmol/L)
Na (mmol/L)
SO4 (mmol/L)
Model Alk. with high Na exchanger
Model Alk. with Ca exchanger
(b)
Model Ca with Na exchanger and sulphate reduction
Model Mg with Na exchanger and sulphate reduction
Model Ca with Na exchanger and sulphate reduction
Model Alkalinity with Na exchanger + sulphate reduction

Table 1

PERIOD	SUPERGROUP	GROUP		FORMATION	AGE [M.A]	MAIN LITHOLOGY
Quartenary	Kalahari	Kalahari		Zambezi	1.8	Sand and Clays
Tertiary				Barotse	65	Sandstone and Quartzites
Early Jurassic	Karoo	Upper	Stormberg Series	Batoka Basalt	225	Basaltic Lavas
				Luena Sandstone		Uniform Graded Sandstone
				Kato Mudstones		Mudstone
			Beaufort Series?	Nkoya Grit	270	Pebbly Sandstone
				Kahare Siltstone		Siltstone
				Machile Sandstone		Quartzose Sandstone
		Lower	Ecca Series	Variegated Mudstone	284	Mudstone
				Luampa Coal		Pebbles, Rock Fragments
Permian			Dwyka Series?	Kado Sandstone	299	Conglomerate/ Muddy Sandstone
Devonian to Ordovician	Pre-Karoo	Pre-Dwkya Series		Likupekupe	488	Arkosic Mudstone

Table 2

ID	Site	DO mg/L	pH	EC µS/cm	TDS g/L	Na mg/L	K mg/L	Ca mg/L	Al mg/L	Si mg/L	Mg mg/L	HCO3 mg/L	Cl mg/L	SO_4 mg/L	Percent Error	Saturation index Cal.	Gyp.	Dol.
Fresh groundwater																		
RV12-2	Machile Basic School	1.7	7.4	482	0.31	32.8	3.60	59.1	0.09	23.4	12.9	270	12.4	14.6	4%	-0.2	-2.5	-0.6
RV12-6	Nyawa Village	5.9	6.8	462	0.30	44.9	2.78	41.7	0.06	25.6	12.5	240	15.6	10.8	2%	-0.8	-2.7	-1.7
RV12-8	Sichifulo School	4.3	6.9	425	0.28	29.1	2.93	41.0	0.04	19.5	20.3	290	2.45	1.20	4%	-0.4	-3.7	-0.8
RV12-9	Simuluwe Village	6	7.1	389	0.25	17.2	3.58	49.8	0.04	22.8	20.6	280	1.89	0.51	5%	-0.5	-3.9	-0.9
RV12-12	Malimba Village	6.8	7.3	558	0.36	51.6	1.48	49.7	0.05	18.3	20.0	300	9.36	5.43	5%	-0.1	-3	-0.3
RV12-16	Katombora Village	4.8	6.7	459	0.30	24.0	0.60	48.1	0.06	45.1	16.7	143	17.0	19.6	8%	-0.9	-2.4	-2
RV12-17	Kachabula Village	5.2	7.2	191	0.12	15.7	0.41	16.6	0.04	23.5	7.35	120	0.00	0.81	4%	-1.1	-4.1	-2.2
RV12-21	Mabwae Village	1.8	6.5	190	0.12	10.3	5.41	24.1	0.01	27.2	2.58	116	5.46	0.00	-0.3%	-1.8	-4.6	-4.2
RV12-22	Moomba Primary	4.2	6.8	64	0.04	2.13	5.15	7.02	0.03	14.8	0.52	24.2	2.50	0.00	10%	-3.4	-5.1	-7.7
RV10	Mulundano Village	6	5.3	16.4	0.01	1.01	1.02	0.96	0.02	8.52	0.27	1.67	2.96	0.00	8%	-3.8	-5.9	-8
RV11	Bwina RHC	7.1	6.9	56.4	0.04	1.20	2.86	7.06	0.03	10.5	0.82	53.5	1.24	0.00	4%	-2.3	-5	-5.5
RV13	Sipula Village	4.7	6.4	67.2	0.04	3.47	2.21	6.48	0.06	26.7	1.06	33.3	0.77	0.00	6%	-2.5	-5.1	-5.5
RV14	Sisibi Basic School	7.6	6.6	16.8	0.01	0.77	2.39	0.47	0.06	11.1	0.33	24.7	1.17	0.00	-3%	-3.7	-6.2	-7.3
RV15	Kabula Village	8.7	6.9	12.8	0.01	0.60	0.75	1.11	0.06	5.1	0.09	46.5	2.29	0.00	1%	-2.9	-5.8	-6.7
RV16	Sianga Village	2.6	6.4	18.6	0.01	0.64	2.75	1.06	0.04	11.1	0.20	17.1	0.00	0.00	3%	-3.6	-5.8	-7.8
RV23	Namatwi Village	6.1	7.4	566	0.37	31.9	5.04	68.3	0.04	30.1	24.3	405	1.76	0.79	2%	0.2	-3.7	0.5
RV29	Mapilelo Village	5	7.5	432	0.28	29.5	5.64	35.5	0.04	24.8	25.3	318	0.00	0.48	1%	-0.1	-4.1	0.1
RV30	Chisu Village	5.6	6.7	82.6	0.05	3.84	1.68	10.0	0.02	11.9	1.68	50	6.39	0.00	-1%	-2.2	-3	-4.9
RV31	Lusinina Village	5.3	7.4	327	0.21	12.0	2.80	55.5	0.04	17.2	3.94	200	6.11	3.82	2%	-0.1	-3	-1.1
RV32	Mushukula Village	4.2	6	28	0.02	0.52	1.72	2.21	0.07	8.4	0.63	15.3	1.04	0.00	1%	-4	-5.5	-8.4
RV09	Salumbwe Village	5.7	6.8	308	0.20	11.1	3.20	34.3	0.03	18.9	14.0	158	5.11	0.38	3%	-0.9	-4.2	-1.9

RV36	Lipumpu Village	5.9	7.2	563	0.37	6.9	4.44	105	0.05	42.7	13.5	398	3.00	3.45	0%	0.1	-2.8	-0.3
RV24	Mwandi Mission	7.5	6.8	580	0.38	13.7	1.52	9.20	0.03	17.3	2.29	65.7	2.68	1.27	5%	-1.7	-4.1	-3.7
RV08	Lutaba Basic School	6.6	7.3	519	0.34	16.4	7.07	69.9	0.03	38.5	18.7	320	3.91	3.20	2%	-0.1	-3.1	-0.2
RV12-11	Sijabala Village	6.7	7.2	825	0.54	60.7	3.66	55.6	0.04	12.2	24.1	0.58	14.2	7.74	8%	-0.1	-2.8	-0.2
RV12-14	Nachilinda School	2.4	6.9	946	0.62	24.6	1.65	27.0	0.03	18.9	4.56	85	2.11	57.1	4%	-0.9	-2.1	-2.2
RV12-10	Siamulunga Village	5.1	7	1156	0.75	71.1	2.99	102	0.09	16.8	57.3	532	38.8	17.2	3%	-0.1	-2.4	-0.1
RV25	Situlu Health Post	8.3	7.6	1017	0.66	256	3.00	1.85	4.10	54.6	0.26	505	42.1	49.1	4%	-1.1	-3.4	-2.9
RV01	Katongo Basic	6.1	7.9	1060	0.69	200	2.70	22.1	0.02	16.0	4.61	135	168	99.1	6%	-0.1	-2.1	-0.6
RV12-3	Katemwa Village	5	7.1	2200	1.43	365	13.7	124.9	0.01	22.0	12.5	396	360	260.0	2%	-0.2	-1.2	-1
Brackish groundwater																		
RV37	Makanga Village	6.1	6.9	2540	1.65	564	6.00	12.4	0.02	42.1	2.56	225	366	458.0	4%	-1.4	-1.9	-3.1
RV26	Adonsi Basic School	4.2	8.3	4710	3.06	1068	5.50	15.4	0.07	12.1	6.45	256	740	1097.3	0%	0.1	-1.6	0.2
Saline groundwater																		
RV12-27	Kasaya Basic School	2.3	6.8	23300	15.15	5279	16.5	770	0.01	31.5	265.5	440	5904	5560.0	0%	0.2	0.1	0.3
RV12-24	Simungoma Basic	6	7.5	16350	10.63	2870	10.4	530	0.57	11.5	164.5	350	2890	3432	6%	0.1	0.8	0.2

Table 3

ID	Borehole name (Upland to topographic low)	Tritium (^{3}H) [TU]	δ13C ‰	^{14}C pmc (uncorrected)	^{14}C pmc (adjusted)	Age (Using Vogel 's Model) Years	DIC (mmol/L)	Water Quality Zone
RV13	Sipula Village	0.03	-21.5	87.9	87.27	M	0.99	Fresh
RV12-2	Machile Basic School	0.29	-20.1	57.3	56.73	3342.84	3.41	Fresh
RV09	Salumbwe Village	0.94	-19.5	93.2	92.16	M	2.83	Transition
RV08	Lutaba Basic School	0.43	-16.0	63.6	62.44	2549.55	3.56	Transition
RV26	Adonsi Basic School	0.00	-20.1	67.8	67.12	1951.88	4.08	Brackish
RV25	Situlu Health Post	0.00	-13.7	66.3	64.79	2244.46	6.92	Brackish
RV37	Makanga Village	0.03	-15.1	102.5	100.45	M	4.62	Brackish
RV12-27	Kasaya Basic School	0.05	-14.9	75.6	74.06	1139.2	8.80	Saline
RV24	Mwandi Basic school	0.71	-12.8	106.2	103.59	M	1.41	Fresh in close proximity (<5 km) to Zambezi River

Table 4

Depth m bgl	CaX2 meq/100g	NaX meq/100g	FeX2 meq/100g	MgX2 meq/100g	AlX3 meq/100g	KX meq/100g	NH4X meq/100g	CEC (sum), meq/100g
14	5.80	2.22	0.00	3.09	1.52	0.27	0.02	12.9
15	10.95	2.31	0.00	2.78	0.00	0.28	0.12	16.5
17	7.29	2.42	0.00	1.22	0.00	0.17	0.20	11.3
19	9.75	2.70	0.00	2.70	0.00	0.23	0.01	15.4
23	8.11	0.53	0.00	0.43	0.00	0.05	0.00	9.13
28	5.36	1.33	0.00	0.59	0.00	0.05	0.18	7.52
30	0.51	0.16	0.00	0.10	0.02	0.06	0.00	0.87
45	9.66	3.42	0.00	3.60	0.00	0.37	0.08	17.1
50	10.90	7.03	0.00	2.51	0.00	0.48	0.09	21.0

Table 5

Depth m bgl	Method	pH	Alkalinity as HCO3 (mg/L)	Cl mg/L	SO_4 mg/L	Na mg/L	K mg/L	Ca mg/L	Mg mg/L	Mn mg/L	CBE (%)	EC µS/cm
14	SPE	6.2	133	747	4697	2840	10.7	82.4	21.0	0.22	3.7%	9766
15	SPE	6.5	242	290	2902	2759	23.4	395.4	69.4	7.66	8.3%	5919
17		7.9	405	185	1199	763	7.3	90.5	17.1	0.34	3.8%	2860
19	SPE	6.2	446	2395	4872	3704	36.5	100.8	31.0	0.02	1.3%	15179
21		5.7	37	5631	6798	6497	33.2	347.3	124.6	0.90	2.0%	25675
23		6.9	131	54	1966	670	16.1	317.9	40.6	0.20	5.4%	3670
28		8.6	882	238	373	622	5.7	29.6	9.8	0.07	2.5%	2389
35	SPE	6.2	334	2043	3876	3465	18.7	136.4	39.1	0.00	6.1%	13560
45	SPE	6.2	144	5884	6795	6938	111.7	304.1	109.2	0.20	4.0%	29686
50	SPE	6.6	1246	1010	1295	1335	10.2	28.2	7.3	0.00	10.9%	5895

Table 6

Initial Water (Solution 1) for high Ca-exchanger	Initial Water (Solution 1) For high Na-exchanger	CEC (eq/L)	SI of Equilibrium Phases (used with initial water)	Initial composition (Solution 2) for high Ca-exchanger	Initial composition (Solution 2) for high Na-exchanger	Equilibrium Phases (saturation index)		Reaction No sulphate reduction	Reaction Sulphate reduction
						Dolomite	Calcite		
pH 7 units: mmol/L HCO_3 10 Ca 5 SO_4 2 Na 100 Cl 100 Mg 2	pH 7 units: mmol/L HCO_3 10 Ca 5 SO_4 2 Na 200 Cl 200 Mg 2	1.2	Dolomite 0 Calcite 0 CO_2 -1.82	pH 6 units: mmol/L HCO_3 3 Ca 1.5 SO_4 0.2 Na 20 Cl 20 Mg 0.2	pH 6 units: mmol/L HCO_3 3 Ca 1.5 SO_4 0.2 Na 200 Cl 200 Mg 0.2	0	0	Gypsum 0.9 moles in 10 steps	Gypsum 0.104 moles in 10 steps
						With sulfate reduction Also: Goethite 0 Pyrite 0			Organic matter 0.070 moles in 10 steps